

# A discrete element analysis of elastic properties of granular materials

X. Q. Gu · J. Yang

Received: 13 October 2012 / Accepted: 10 January 2013 / Published online: 23 January 2013  
© Springer-Verlag Berlin Heidelberg 2013

**Abstract** The elastic properties of a regular packing of spheres with different tolerances were evaluated using the discrete element method to elucidate the mechanisms behind the discrepancies between laboratory experiments and theoretical predictions of the classic Hertz-Mindlin contact law. The simulations indicate that the elastic modulus of the packing is highly dependent on the coordination number and the magnitude and distribution of contact normal forces, and this dependence is macroscopically reflected as the influence of confining pressure and void ratio. The increase of coordination number and the uniformity of contact normal forces distribution with increasing confining pressure results in the stress exponent  $n$  for elastic modulus being higher than  $1/3$  as predicted by the Hertz-Mindlin law. Furthermore, the simulations show that Poisson's ratio of a granular packing is not a constant as commonly assumed, but rather it decreases as confining pressure increases. The variation of Poisson's ratio appears to be a consequence of the increase of the coordination number rather than the increase of contact normal forces with confining pressure.

**Keywords** Elastic moduli · Granular material · Poisson's ratio · Pressure dependence

## 1 Introduction

It is well agreed in soil mechanics that the elastic shear modulus  $G_0$  or Young's modulus  $E_0$  of a dry granular soil (e.g. sand and gravel) highly depends on void ratio ( $e$ ) and confining pressure ( $P$ ) and can be expressed by a general form as follows [1,2]:

$$G_0 \text{ (or } E_0) = AF(e) \left( \frac{P}{P_a} \right)^n \quad (1)$$

where  $A$  is a constant reflecting soil type, grain properties and fabric,  $P_a$  is a reference stress typically taking a value of 98 kPa,  $n$  is the stress exponent reflecting the effect of confining pressure, and  $F(e)$  is a void ratio function reflecting the effect of soil density.

Given their vital importance in geotechnical engineering applications, extensive experimental studies have been carried out in the past decades to estimate the elastic properties for various granular soils under a range of conditions [3–8]. The experimental results have consistently showed that  $n$  value for shear modulus generally ranges between 0.4 and 0.6, which is always larger than the value of  $1/3$ , predicted by the classical Hertz-Mindlin contact law [9, 10]. Several studies on quartz sand also showed that  $n$  value for shear modulus increases with increasing the coefficient of uniformity of sand [11] and with increasing void ratio of the assembly [12].

There are currently two major explanations for the discrepancy of  $n$  values between experimental data and theoretical prediction. The first explanation attributes it to the discrepancy between the Hertz-Mindlin contact law and the actual contact condition, thus leading to several modified contact laws. For example, Goddard [13] proposed a contact law for conical contacts of which the stress exponent  $n$  changes from  $1/2$  to  $1/3$  when the confining pressure exceeds a transition value. However, there is experimental evidence that values

---

X. Q. Gu  
Department of Geotechnical Engineering,  
Tongji University, Shanghai, China

X. Q. Gu · J. Yang (✉)  
Department of Civil Engineering,  
The University of Hong Kong, Pokfulam, Hong Kong  
e-mail: junyang@hku.hk

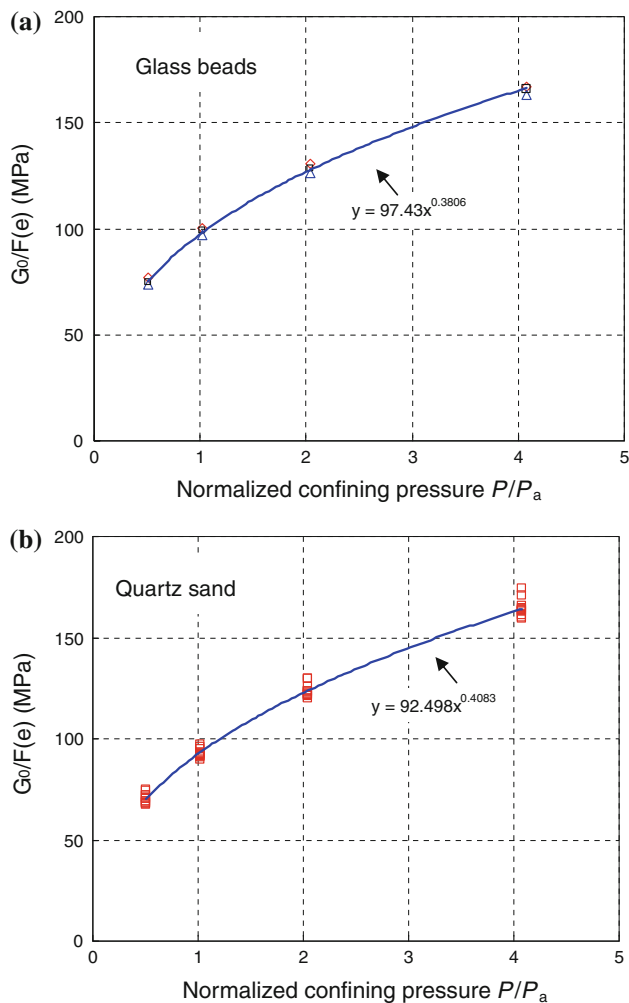


**Fig. 1** Measured elastic shear modulus versus normalized confining pressure (data from [8, 12]): **a** glass beads; **b** quartz sand

of  $n$  for assemblies of spherical steel balls and glass beads are similar to that for angular sands [8, 9, 14, 15]. An example is here given in Fig. 1, showing laboratory measurements of the elastic shear modulus of spherical glass beads and quartz sand at a range of pressures, obtained by Yang and Gu [8, 12] using the resonant column technique. Yimsiri and Soga [16] modified the Hertz-Mindlin contact law by accounting for grain surface roughness and predicted an  $n$ -value of 0.55. With this modified contact model, Poisson's ratio is predicted to increase as confining pressure increases, which is however in contrast to the experimental observations [5, 17, 18].

The second possible explanation for the discrepancy is the change of fabric during the increase of confining pressure that causes an additional increase in stiffness [8, 19]. In the experiments of Duffy and Mindlin [9] on face-centered cubic packings of steel balls, two types of steel balls were used, including high tolerance spheres with diameters  $1/8 \pm (10 \times 10^{-6})$  in. (HTS) and low tolerance ones with diameters  $1/8 \pm (50 \times 10^{-6})$  in. (LTS). It is interesting to

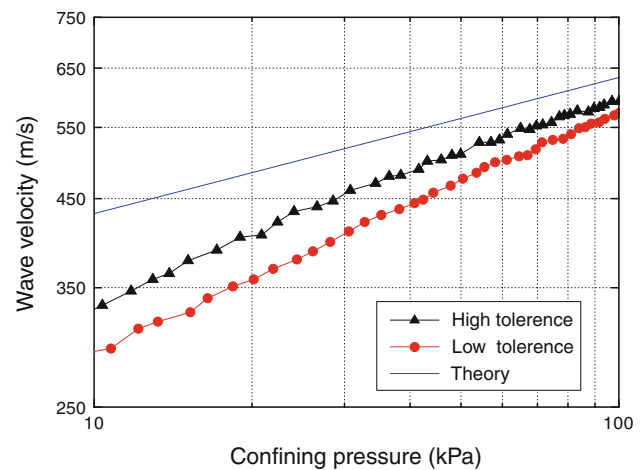


**Fig. 2** Longitudinal wave velocity versus confining pressure (data from [9])

note that the measured longitudinal wave velocity in the LTS is much lower than that in the HTS, but both are significantly lower than the theoretical prediction, particularly at low confining pressures (Fig. 2). Meanwhile, the stress exponent  $n$  for elastic modulus from the experiments is higher than the predicted value  $1/3$ , especially in the LTS. Duffy and Mindlin speculated that the discrepancy was probably due to the evolution of contacts between the steel balls. However, how the contact number evolves and how it affects the stiffness are not yet well understood.

For an isotropic elastic continuum, shear modulus and Young's modulus can be linked by Poisson's ratio  $\nu$  as the following:

$$\nu = \frac{E_0}{2G_0} - 1 \quad (2)$$

Laboratory experiments on granular soils showed that Poisson's ratio decreases as confining pressure increases and as void ratio decreases [5, 18]. It was also reported that Poisson's ratio of sand depends on the coefficient of uniformity [7]. However, based on the Hertz-Mindlin contact law, Chang et al. [20] obtained Poisson's ratio for a random isotropic packing as follows:

$$\nu = \frac{\nu_g}{2(5 - 3\nu_g)} \quad (3)$$

where  $\nu_g$  is the Poisson's ratio of the grain. Equation (3) predicts that Poisson's ratio of a granular material is an extremely small constant (e.g.  $\nu = 0.037$  for  $\nu_g = 0.30$ ), which is inconsistent with experimental data that Poisson's ratio of glass beads and quartz sand has typical values of 0.2–0.3 and varies with confining pressure [18].

This paper presents a numerical study aimed to address the above issues on elastic properties of granular materials that are of fundamental importance. By means of a grain-scale

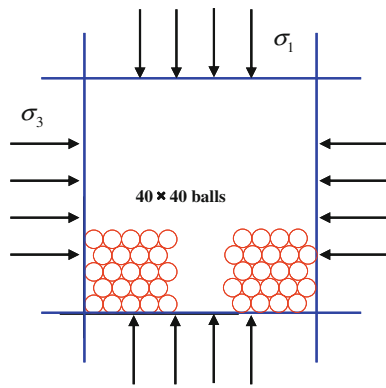


Fig. 3 Regular packing (40 × 40 balls) used in DEM simulations

modeling technique known as discrete element method (DEM), the elastic properties of a regular packing of spheres with different tolerances are evaluated. The microstructure of the packing during the increase of confining pressure, including contact number, contact normal forces and their evolution, is investigated. Particularly, the link between the microstructure and the macroscopic elastic properties is explored to elucidate the mechanisms behind the pressure dependence of elastic properties.

## 2 Numerical simulation

The DEM simulations were conducted using PFC<sup>2D</sup> [21] on a regular packing with 40 × 40 balls (Fig. 3), whose nominal diameter (*D*) was set to be 2.0 mm. Similar to the physical tests of Duffy and Mindlin [9], five tolerances (*T<sub>r</sub>*) of the balls were considered, namely *T<sub>r</sub>* = 0, 0.008, 0.04, 0.2 and 1%. For each tolerance, balls with diameters in the range of *D*(1 ± *T<sub>r</sub>*) were randomly generated to form a uniform distribution. The Hertz-Mindlin contact law was adopted to describe the force-dependent contact stiffness. The basic parameters for the DEM simulations are summarized in Table 1.

Following the procedure similar to laboratory experiment [22], the packing was first isotropically consolidated to different confining pressures and at each confining pressure a drained biaxial test was then conducted at very small strain. In doing that, a small axial strain increment Δε<sub>1</sub> was applied, while the radial stress σ<sub>3</sub> was kept constant by servo control until the shear strain Δγ = Δε<sub>1</sub> - Δε<sub>3</sub> reached 10<sup>-6</sup> (Fig. 3).

Under this condition, the elastic Young’s modulus *E*<sub>1</sub>, shear modulus *G*<sub>13</sub> and Poisson’s ratio ν<sub>13</sub> can be determined as follows:

$$E_1 = \frac{\Delta\sigma_1}{\Delta\varepsilon_1} \tag{4}$$

$$G_{13} = \frac{\Delta\tau}{\Delta\gamma} = \frac{\Delta\sigma_1/2}{\Delta\varepsilon_1 - \Delta\varepsilon_3} \tag{5}$$

$$\nu_{13} = -\frac{\Delta\varepsilon_3}{\Delta\varepsilon_1} \tag{6}$$

Note that the first number in the subscript denotes the loading direction.

## 3 Results and discussion

### 3.1 Macroscopic elastic properties

Figure 4 shows typical stress-strain curves for the specimen of *T<sub>r</sub>* = 0.2% at the confining pressure (*P*) of 100 kPa. Obviously, the specimen behaves in a linear manner at this small strain level. Given the stress-strain curves at different confining pressures, the elastic Young’s modulus *E*<sub>1</sub> and shear modulus *G*<sub>13</sub> can be determined as a function of *P*, as shown in Fig. 5 for all five specimens. The void ratios of the specimens at different confining pressures were also determined and summarized in Table 2.

A comparison of Figs. 2 and 5 shows a strong similarity between simulations and experimental data in terms of the pressure dependence of elastic modulus. At a constant confining pressure, both shear modulus and Young’s modulus decreases as *T<sub>r</sub>* increases. Furthermore, for both shear modulus and Young’s modulus, the rate of variation with pressure tends to decrease as pressure increases, especially for specimens with high *T<sub>r</sub>* values at low pressures. Note that at a given confining pressure, the specimens of different tolerances have almost the same void ratios but significantly different values of elastic moduli, implying that the fabric of the packing in terms of number of contacts and contact forces plays an important role.

For better illustration, the moduli in the pressure range of 10–1,000 kPa are fitted by Eq. (1) (modulus in MPa and pressure in kPa) and the best-fit parameters are given in Table 3. It is interesting to note that, although the Hertz-Mindlin contact law was used in the simulations, all *n* values are larger than

Table 1 Parameters for simulations

Wall stiffness	Rigid	No. of particles	1,600
Wall-particle friction	0	Particle diameter	2.0 mm (nominal)
Contact law	Hertz-Mindlin	Particle density	2,600 kg/m <sup>3</sup>
Particle shape	Spherical	Shear modulus and Poisson’s ratio of particles	29 GPa; 0.15
Thickness of sample	2.0 mm	Inter-particle friction coefficient	0.5

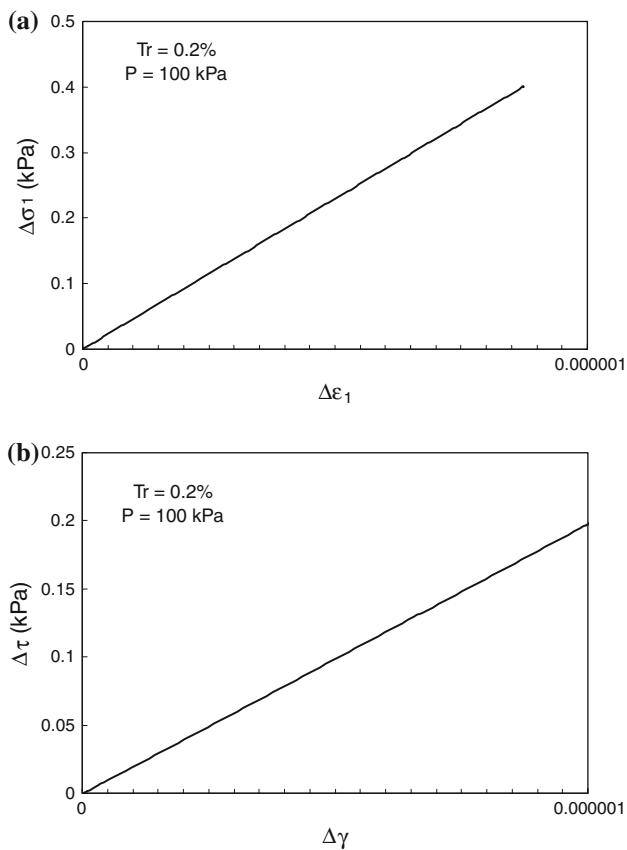


**Fig. 4** Stress-strain curves of a regular packing of spheres with  $T_r = 0.2\%$  at confining pressure of 100 kPa: **a**  $\Delta\sigma_1 - \Delta\varepsilon_1$  and **b**  $\Delta\tau - \Delta\gamma$

1/3 except for the case of  $T_r = 0\%$ , for which the stress exponent is almost exactly 1/3, and that the stress exponent  $n$  generally increases as  $T_r$  increases. This result indicates that the stress exponent not only reflects the stress-dependent contact stiffness, but also the fabric of the packing associated with contact number and contact force. Moreover, for each packing the stress exponent  $n$  for shear modulus is always larger than that for Young’s modulus, suggesting that the former increases faster than the latter as confining pressure increases.

Figure 6 presents the calculated values of Poisson’s ratio  $\nu_{13}$  at different pressures for the specimens with different tolerances. Evidently, Poisson’s ratio decreases with increasing confining pressure except for the case of  $T_r = 0\%$  where it

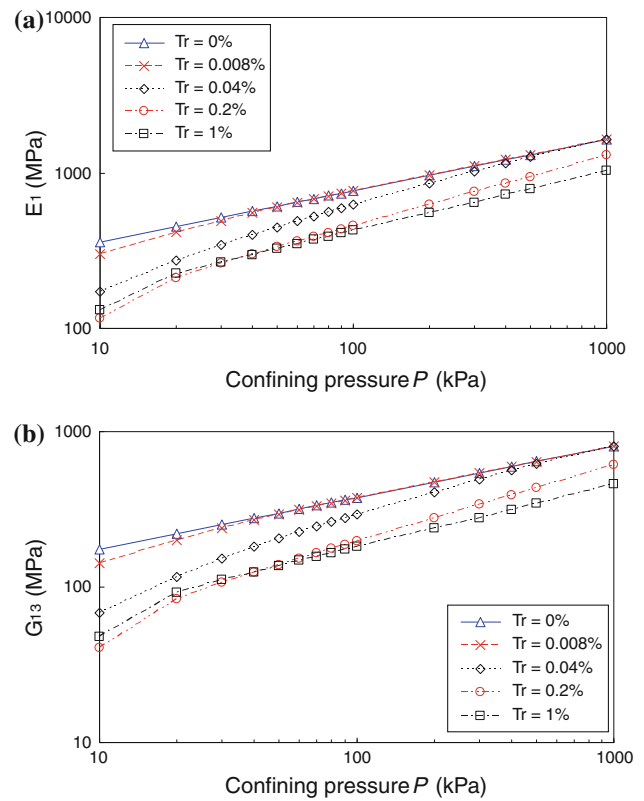


**Fig. 5** Variation of elastic modulus with confining pressure: **a**  $E_1$  and **b**  $G_{13}$

is a constant. The values of Poisson’s ratio are significantly different at different  $T_r$  values, especially at low confining pressures. Figure 6 suggests that besides confining pressure, there are other influencing factors for Poisson’s ratio, as will be discussed later.

### 3.2 Macroscopic characteristics

Due to the particulate nature, contacts bear and transfer the loads in a granular material. Therefore, the contact number, contact force and its distribution are all expected to play an important role in macroscale stiffness. Here, two conceptual models are proposed (Fig. 7) to illustrate the importance of contact number and the distribution of contact force. In the

**Table 2** Void ratios and coordination numbers of packings under various conditions

$P$ (kPa)	$e, CN$				
	$T_r = 0\%$	0.008%	0.04%	0.2%	1%
10	0.121, 5.97	0.121, 5.50	0.121, 3.92	0.122, 3.53	0.127, 3.71
50	0.121, 5.97	0.121, 5.96	0.121, 4.83	0.122, 3.90	0.127, 3.79
100	0.121, 5.97	0.120, 5.97	0.120, 5.18	0.120, 4.10	0.127, 3.85
500	0.120, 5.97	0.120, 5.97	0.120, 5.93	0.120, 4.70	0.126, 4.03
1,000	0.119, 5.97	0.119, 5.97	0.119, 5.97	0.120, 5.06	0.125, 4.20

**Table 3** Fitting results of elastic moduli using Eq. (1)

$T_r$ (%)	$E_1$		$G_{13}$	
	$AF(e)$	$n$	$AF(e)$	$n$
0	762.0	0.332	373.5	0.332
0.008	743.7	0.359	363.0	0.364
0.04	596.0	0.478	276.5	0.519
0.2	443.5	0.490	189.3	0.543
1	407.9	0.413	174.6	0.443

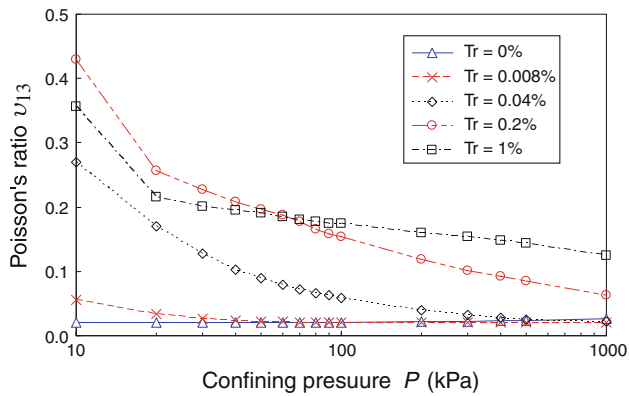


**Fig. 6** Variation of Poisson's ratio with confining pressure

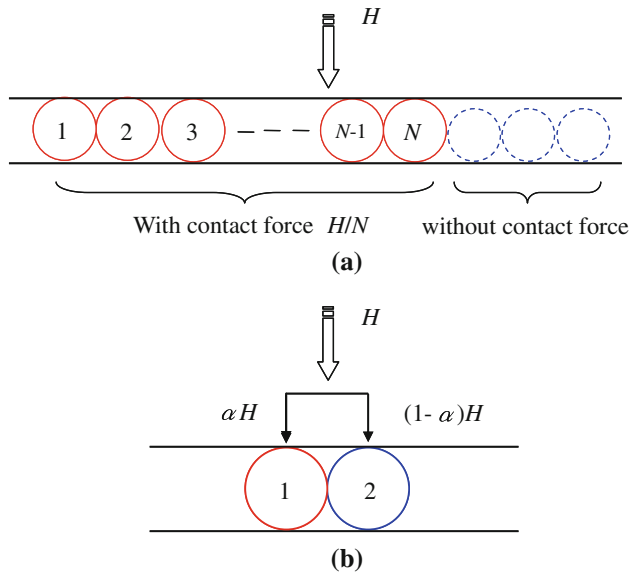


**Fig. 7** Models illustrating the importance of (a) contact number (b) distribution of contact forces

first model, the external force  $H$  is evenly distributed to  $N$  identical particles and the stiffness of the assembly is found to be proportional to  $H^{1/3}$  and  $N^{2/3}$  when the Hertz-Mindlin contact law is used. It indicates that for a constant external force (or pressure), the stiffness of the assembly increases as contact number  $N$  increases. In the second model (Fig. 7b),

**Table 4** Effect of contact force distribution on stiffness

$\alpha$	$k_1/K_{\text{even}}$	$k_2/K_{\text{even}}$	$K/K_{\text{even}}$
0.5	0.50	0.50	1.00
0.4	0.45	0.55	0.99
0.3	0.39	0.59	0.98
0.2	0.32	0.63	0.95
0.1	0.22	0.67	0.89
0	0.00	0.71	0.71

$k_1$  and  $k_2$  contact stiffness of particle 1 and 2, respectively,  $K$  the overall stiffness,  $K_{\text{even}}$  the overall stiffness at even distribution of the contact force

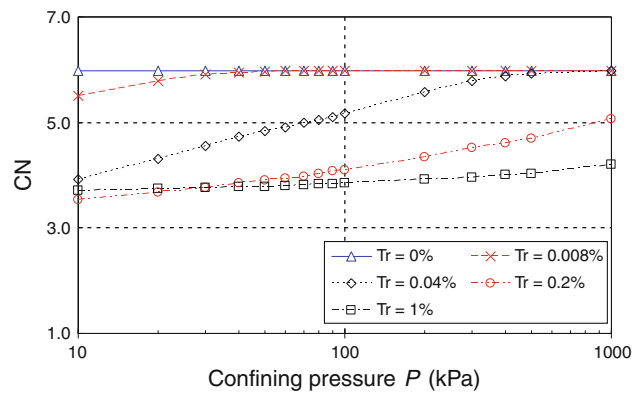


**Fig. 8** Variation of coordination number (CN) with confining pressure

the external force  $H$  is distributed to two contacts and the uniformity of distribution is controlled by a factor  $\alpha$ . The stiffness of the assembly decreases continuously as the uniformity of force distribution decreases (i.e.  $\alpha$  decreases), as seen in Table 4.

Given the above consideration based on the conceptual models, the evolution of coordination number  $CN$  (i.e. the average number of contacts per particle) with increasing confining pressure  $P$  was examined for all specimens of different tolerances, as shown in Fig. 8. Note that only the particles with more than two contacts were used to calculate  $CN$ , while all particles were used to evaluate the void ratio [23]. As seen in Fig. 8, for  $T_r = 0\%$ ,  $CN$  keeps constant as pressure increases and the value of stress exponent  $n$  for elastic moduli is  $1/3$ , exactly the same as that predicted by the Hertz-Mindlin contact law. However, for  $T_r = 0.008$  and  $0.04\%$ ,  $CN$  increases as pressure increases until all the contacts make. For  $T_r = 0.2$  and  $1.0\%$ , the value of  $CN$  is well below the maximum, even at the pressure level as high as  $1,000\text{ kPa}$ . Figure 8 provides strong evidence showing that the value of stress exponent  $n$  is closely related to the evolution of  $CN$ .

It should be emphasized that the coordination number correlates well with the magnitude of contact force at a constant confining pressure. To make this point, the average contact normal force,  $F_{\text{avg}}$ , was normalized by confining pressure,

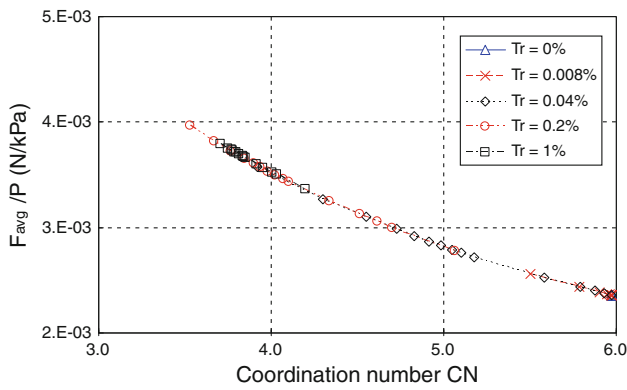


**Fig. 9** Relation between normalized average contact normal force and coordination number

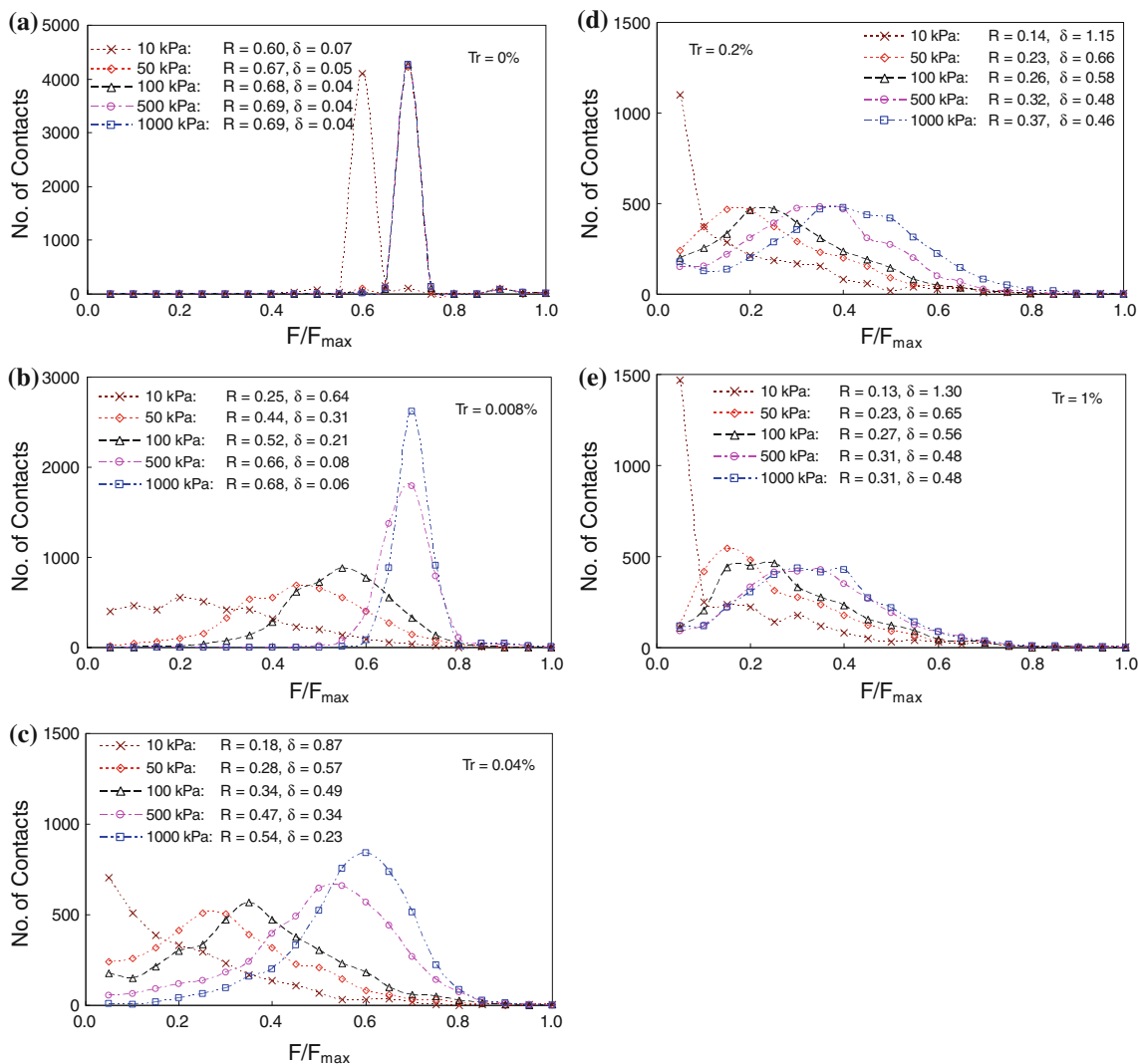
$P$ , and then was presented as a function of  $CN$ , as shown in Fig. 9. Obviously, the value of  $F_{avg}/P$  decreases as coordination number increases and the relationship is unique

irrespective of the degree of tolerance. In addition to the magnitude, the distribution of contact normal forces is also thought to be a key factor because it determines the distribution of contact stiffness. Figure 10 shows the distribution of contact normal force  $F$  normalized by the maximum contact normal force  $F_{max}$  at different levels of confining pressure. In Fig. 10,  $R$  is the ratio of  $F_{avg}$  to  $F_{max}$ , and  $\delta$  is the standard deviation of the normalized contact normal forces, given by

$$\delta = \sqrt{\frac{\sum_{i=1}^N (F_i/F_{avg} - 1)^2}{N}} \quad (7)$$

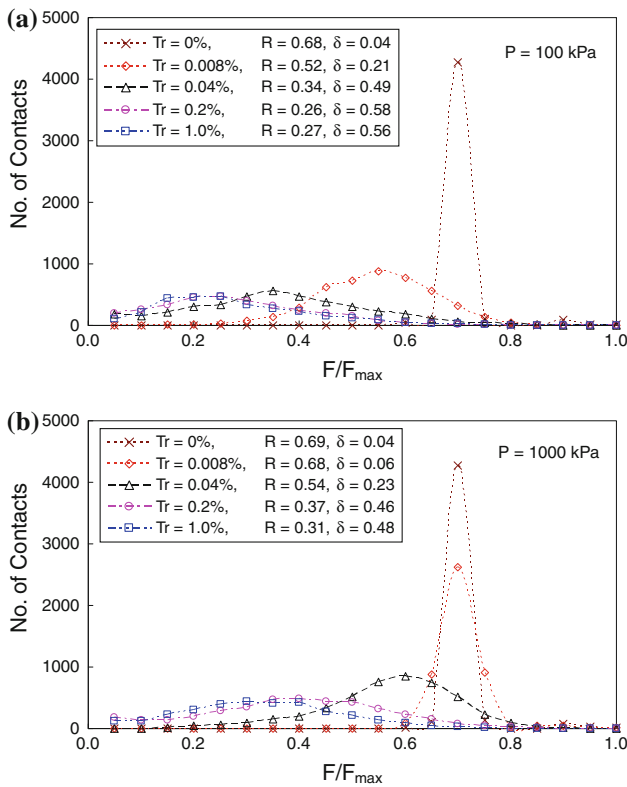
where  $F_i$  is the magnitude of the normal force at the  $i$ th contact and  $N$  is the total number of contacts.

Figure 10 indicates that even for a regular packing of spheres under isotropic confinement, the distribution of contact normal forces is far from uniform distribution, especially at low confining pressures. As confining pressure increases,



**Fig. 10** Statistics of number of contacts based on normalized contact normal force for packings of different  $T_r$  values: **a** 0%, **b** 0.008%, **c** 0.04%, **d** 0.2%, **e** 1%





**Fig. 11** Statistics of number of contacts based on normalized contact normal force for packings of different  $T_r$  values: **a**  $P = 100$  kPa, **b**  $P = 1,000$  kPa

the curves shift to right and the values of  $R$  increase while  $\delta$  decreases, indicating that the distribution of contact normal forces becomes more uniform. For better illustration, the distributions of contact normal forces for specimens with different  $T_r$  values are compared, as shown in Fig. 11. Apparently, at a constant pressure the distribution of contact normal forces is more uniform in the specimen with a smaller  $T_r$  value.

### 3.3 Links between macroscopic properties and microscopic characteristics

Bearing in mind the analysis of the conceptual model in Fig. 7a, the elastic shear modulus and Young's modulus are normalized by  $P^{1/3}$  and then plotted against  $CN^{2/3}$ , as shown in Fig. 12. It is interesting to note that there is a good correlation between normalized modulus and  $CN^{2/3}$ , except at low values of  $CN$  (i.e. low levels of pressure) corresponding to non-uniform distribution of contact normal forces, as indicated by Figs. 10 and 11.

To account for the non-uniform distribution of contact normal forces, each contact is multiplied by a factor defined as  $(F_i/F_{avg})^{1/3}$ , and the coordination number is re-calculated based on the weighted contact and denoted as  $CN'$ . It is strik-

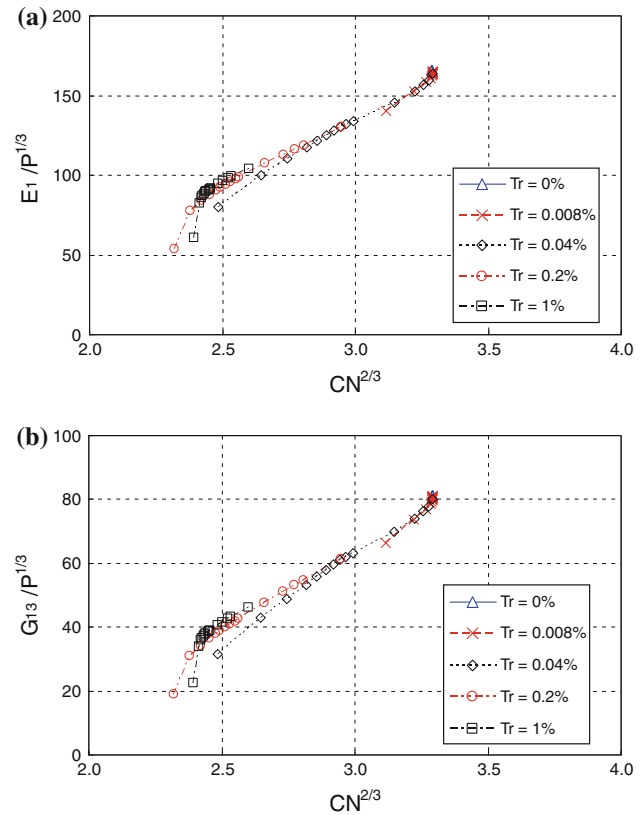


**Fig. 12** Relation between elastic modulus and coordination number: **a**  $E_1/P^{1/3}$  versus  $CN^{2/3}$ ; **b**  $G_{13}/P^{1/3}$  versus  $CN^{2/3}$  (modulus in MPa, pressure in kPa)

ing that the normalized elastic modulus linearly increases with  $CN^{2/3}$ , as shown in Fig. 13. These results suggest that the coordination number and the distribution of contact normal forces are the predominant factors for the elastic stiffness of granular materials. Recalling the physical tests by Duffy and Mindlin [9], the difference between the specimens with high and low tolerance steel balls can be reasonably explained as the difference of coordination number and distribution of contact normal forces, although their void ratios are nearly the same.

Meanwhile, it is found that Poisson's ratio decreases as  $CN^{2/3}$  increases, as shown in Fig. 14. By comparing Figs. 6 and 14, it can be concluded that Poisson's ratio of a granular packing is essentially dependent on the coordination number. A probable explanation for the laboratory observation that Poisson's ratio decreases as void ratio decreases or as confining pressure increases is the increase of coordination number due to the increase of confining pressure or packing density.

## 4 Conclusions

The elastic properties of a regular packing of spheres with different tolerances were numerically evaluated by DEM modeling, and particular effort was made to link the macroscopic

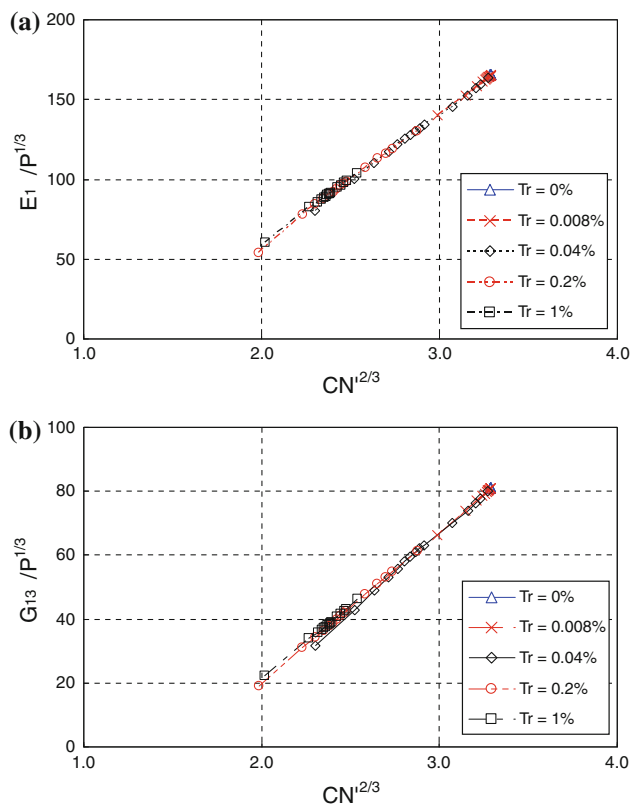


**Fig. 13** Relation between elastic modulus and modified coordination number: **a**  $E_1/P^{1/3}$  versus  $CN'^{2/3}$ ; **b**  $G_{13}/P^{1/3}$  versus  $CN'^{2/3}$  (modulus in MPa, pressure in kPa)

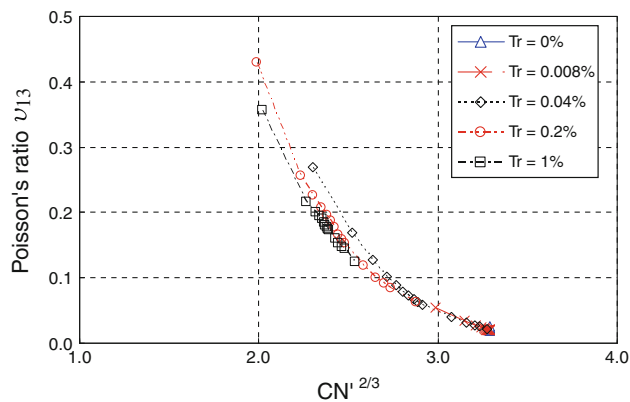


**Fig. 14** Relation between Poisson's ratio and modified coordination number  $CN'^{2/3}$

elastic properties with the microstructure of the granular packing to elucidate the mechanisms involved. The main findings of this study can be summarized as follows.

- (a) The stress exponent  $n$  for both shear modulus and Young's modulus of the packing of spheres with  $T_r = 0\%$  is  $1/3$ , exactly same as the prediction by the Hertz-Mindlin contact law. All other packings with

non-zero  $T_r$  values show, however, that the  $n$  value is greater than  $1/3$  and it generally increases as  $T_r$  increases. This result suggests that the stress exponent reflects not only the stress-dependent contact stiffness but also the evolution of microstructure during the increase of confining pressure.

- (b) At the particle level, both shear modulus and Young's modulus are highly dependent on the coordination number and the magnitude and distribution of contact normal forces. With increasing confining pressure, the coordination number increases and the distribution of contact normal force becomes more uniform, which lead to further increase of elastic moduli in addition to that caused by the increase of the magnitude of contact normal forces.
- (c) Poisson's ratio generally decreases with increasing confining pressure, except for the case of packing with  $T_r = 0\%$  where it is a constant. Given a confining pressure, the values of Poisson's ratio are significantly different for packings with different  $T_r$  values. At the particle level, this phenomenon appears to result from the increase of coordination number rather than the increase of contact normal forces with the increase of confining pressure.
- (d) By defining a weighted coordination number  $CN'$ , a unique linear relationship is found between  $CN'^{2/3}$  and the elastic moduli normalized by  $P^{1/3}$ , and this relationship holds for all packings with different tolerance spheres and under a range of confining pressures.

**Acknowledgments** The work presented in this paper was supported by the University of Hong Kong through the Seed Funding for Basic Research scheme (11159098) and the Outstanding Young Researcher Award scheme (2006–2007). This support is gratefully acknowledged.

## References

- Hardin, B.O., Richart, F.E.: Elastic wave velocities in granular soils. *J. Soil Mech. Found. Eng. Div.* **89**(SM1), 39–56 (1963)
- Richart, F.E., Hall, J.R., Woods, R.D.: *Vibrations of Soils and Foundations*. Prentice-Hall, Englewood Cliffs (1970)
- Hardin, B.O., Drnevich, V.P.: Shear modulus and damping in soil: Measurement and parameter effects. *J. Soil Mech. Found. Div.* **98**(7), 603–624 (1972)
- Iwasaki, T., Tatsuoka, F.: Effect of grain size and grading on dynamic shear moduli of sand. *Soils Found.* **17**(3), 19–35 (1977)
- Kokusho, T.: Cyclic triaxial test of dynamic soil properties for wide strain range. *Soils Found.* **20**(2), 45–60 (1980)
- Stokoe, K.H.I.I., Hwang, S.K., Lee, J.N.-K.: Effects of various parameters on the stiffness and damping of soils at small to medium strains. *Proc. First Int. Conf. Prefail. Deformat. Charact. Geomater.* **2**, 785–816 (1995)
- Wichtmann, T., Triantafyllidis, T.: On the influence of the grain size distribution curve on P-wave velocity, constrained elastic modulus  $M_{\max}$  and Poisson's ratio of quartz sands. *Soil Dyn. Earthq. Eng.* **30**, 757–766 (2010)



8. Yang, J., Gu, X.Q.: Shear stiffness of granular material at small strain: does it depend on grain size? *Géotechnique* **63**(2), 165–179 (2013)
9. Duffy, J., Mindlin, R.D.: Stress-strain relations and vibrations of a granular medium. *J. Appl. Mech.* **24**, 585–593 (1956)
10. Petrakis, E., Dobry, R.: Micromechanical Modeling of Granular Soil at Small Strain by Arrays of Elastic Spheres. Report CE-87-02, Dept. Civil Eng., Rensselaer Polytechnic Institute, Troy, NY (1987)
11. Wichtmann, T., Triantafyllidis, Th: Influence of the grain-size distribution curve of quartz sand on small strain shear modulus  $G_{\max}$ . *J. Geotech. Geoenviron. Eng.* **135**(10), 1404–1418 (2009)
12. Yang, J., Gu, X.Q.: Dynamic shear modulus of dry sand: effect of test method. In: Proceedings of the 14th European Conference on Earthquake Engineering, Ohrid, Macedonia (2010)
13. Goddard, J.D.: Nonlinear elasticity and pressure-dependent wave speeds in granular media. *Proc. R. Soc. Lond.* **430**, 105–131 (1990)
14. Chen, Y.-C., Ishibashi, I., Jenkins, J.T.: Dynamic shear modulus and fabric: Part I, depositional and induced anisotropy. *Géotechnique* **38**(1), 25–32 (1988)
15. Santamarina, J.C., Cascante, G.: Effect of surface roughness on the wave propagation parameters. *Géotechnique* **48**(1), 129–136 (1998)
16. Yimsiri, S., Soga, K.: Effect of surface roughness on small-strain modulus: Micromechanics view. Proc. 2nd Int. Symp. Prefail. Deform. Charact. Geomater. **1**, 597–602 (1999)
17. Kumar, J., Madhusudhan, B.N.: Effect of relative density and confining pressure on Poisson ratio from bender-extender element tests. *Géotechnique* **60**(7), 561–567 (2010)
18. Gu, X.Q.: Dynamic Properties of Granular Materials at the Macro and Micro Scales. PhD thesis, The University of Hong Kong, Hong Kong (2012)
19. McDowell, G.R., Bolton, M.D.: Micro mechanics of elastic soil. *Soils Found.* **41**(6), 147–152 (2001)
20. Chang, C.S., Misra, A., Sundaram, S.S.: Properties of granular packing under low amplitude cyclic loading. *Soil Dyn. Earthq. Eng.* **10**(4), 201–211 (1991)
21. Itasca: User's manual for PFC<sup>2D</sup>. Itasca Consulting Group, Inc., Minneapolis (2005)
22. Hoque, E., Tatsuoka, F.: Effects of stress ratio on small-strain stiffness during triaxial shearing. *Géotechnique* **54**(7), 429–439 (2004)
23. Thornton, C.: Numerical simulations of deviatoric shear deformation of granular media. *Géotechnique* **50**(1), 43–53 (2000)